EPJ manuscript No.
(will be inserted by the editor)

Isentropic thermodynamics and scalar mesons properties near the QCD critical end point

Pedro Costa [a]

CFisUC, Department of Physics, University of Coimbra, P-3004 - 516 Coimbra, Portugal

Received: date / Revised version: date

Abstract. We investigate the QCD phase diagram and the location of the critical end point (CEP) in the SU(2) Polyakov−Nambu−Jona-Lasinio model with entanglement interaction giving special attention to the π and σ-mesons properties, namely the decay widths $\sigma \to \pi\pi$, for several conditions around the CEP: we focus on the possible $\sigma \to \pi\pi$ decay along the isentropic trajectories close to the CEP since the hydrodynamical expansion of a heavy-ion collision fireball nearly follows trajectories of constant entropy. It is expected that the type of transition the dense medium goes through as it expands after the thermalization determines the behavior of this decay. It is shown that no pions are produced from the sigma decay in the chirally symmetric phase if the isentropic lines approach the first order line from chemical potentials above it. Near the CEP or above the $\sigma \to \pi\pi$ decay is possible with a high decay width.

1 Introduction

The possible existence of the critical end point (CEP) and its implications to the investigation of the QCD phase diagram is a very timely topic that has drawn the attention of the physics community.

From the experimental point of view, the location of the CEP is one major goal of several heavy ion collisions (HIC) programs. At RHIC, the Beam Energy Scan (BES-I) program, ongoing since 2010, is looking for the experimental signatures of the first-order phase transition and the CEP by colliding Au ions at several energies [4]. Also the STAR Collaboration presented their measurements on the moments of net-charge multiplicity distributions, which can provide relevant information on the freeze-out conditions, in order to clarify the existence of the CEP, but no definitive conclusions were possible and future measurements with high statistics data will be needed [5]. With the upcoming BES-II program, it is expected that, if the CEP exists at a baryonic chemical potential below 400 MeV, it can provide data on fluctuation and flow observables which should yield quantitative evidence for the presence of the CEP.

Meanwhile, the NA49 program at CERN SPS has also investigated the CEP's location in nuclear collisions at 158A GeV [6]: the analysis for $\pi^+\pi^-$ pairs with an invariant mass very close to the two-pion threshold has been performed in [6]. This sector is important because it may reveal critical fluctuations of the sigma component in a hadronic medium, even if the σ- meson has no well-defined vacuum state. In spite of a sizable effect of $\pi^+\pi^-$ pair fluctuations with critical characteristics found in Si + Si collisions at 158A GeV, this effect could not be directly related to the presence of the CEP. Now, the NA61/SHINE program is devoted to the search for the CEP and to investigate the properties of the onset of deconfinement in light and heavy ion collisions [7]. So far, no definitive results were found about the existence of the CEP.

In the next years, FAIR facility at GSI and the Nuclotron-based Ion Collider Facility at JINR (NICA) will extend the CEP's search to even higher μ_B and definitive conclusions concerning its existence and location are expected (for a review on the experimental search of the CEP see [8]).

It is known that the location of the CEP is affected by several conditions like the isospin or strangeness content of the medium [9], the presence of an external magnetic field [9,10] or the role of the vector interaction in the medium [10,11]. The determination of the CEP's location will set stringiest constraint on effective models.

Probes like diphoton and dipion productions are important tools for the search of the CEP. In this work we will focus on the dipion production. However, concerning the diphoton production, it is important to point out that the enhancement of photon pair production rate at threshold should also belong to the set of observable effects for the investigation of chiral symmetry restoration in ultra-relativisitc HIC experiments. Indeed, in [2] it was shown that the process $\bar{q}q \to \gamma\gamma$, which occurs due to the formation of mesonic resonances, leads to an enhancement of photon pairs with invariant mass equal to the thermal pion mass. On the other hand, the photon pair production by pion annihilation ($2\pi \to 2\gamma$) at the chiral phase transition was investigated in [1] where the following results were found: a strong enhancement of the cross section for the pion annihilation process when compared with the vacuum case; the calculation of the photon pair production

[a] email: pcosta@uc.pt

rate as function of the invariant mass showed a strong enhancement and narrowing of the sigma meson resonance at threshold. Both results are directly related to the chiral symmetry restoration. However, the $\pi^0 \to \gamma\gamma$ decay gives a strong background contribution making difficult the observation of these effects at high energy collisions. One strength of NICA facility, namely the Baryonic Matter at Nuclotron (BM@N) experiment, concerns the diphoton production: the electromagnetic calorimeters that will be used have large acceptance and high resolution allowing to investigate the invariant mass spectra of $\gamma\gamma$ pairs in the wide range at different energies and transverse momenta of pairs [3].

The measurement of the $\sigma \to \gamma\gamma$ decay is also relevant because of the small final state interactions [12]. Finally, measuring the $\sigma \to 2\pi^0 \to 4\gamma$ [13] can avoid the possible background from the $\rho-$ meson inherent to the $\pi^+\pi^-$ measurement.

In the present work we investigate the π and σ-mesons masses and the decay width of $\sigma \to \pi\pi$ for several conditions around the CEP, namely along the isentropic trajectories close to the CEP because it is likely that the system expands nearly isentropically after the thermalization.

2 Model and formalism

In this work we consider the two-flavor Polyakov−Nambu−Jona-Lasinio (PNJL) model which Lagrangian is

$$\mathcal{L} = \bar{q}(i\gamma^\mu D^\mu - \hat{m}_0)q + G_S\left[(\bar{q}q)^2 + (\bar{q}i\gamma_5\boldsymbol{\tau}q)^2\right] + \mathcal{U}\left(\Phi[A], \bar{\Phi}[A]; T\right). \quad (1)$$

Here, $q = (u, d)^T$ represents a quark field with 2-flavors, $\hat{m}_0 = \mathrm{diag}_f(m_u, m_d)$ is the corresponding (current) mass matrix, with $m_u = m_d = m_0$ (to keep the isospin symmetry) and $\boldsymbol{\tau}$ is a Pauli matrix which acts in flavor space.

The quarks are coupled to the gauge sector *via* the covariant derivative, $D^\mu = \partial^\mu - iA^\mu$, and the order parameter of $\mathbb{Z}_3$ symmetric/broken phase transition in pure gauge is the Polyakov loop Φ (see details in [14,15]).

The pure gauge sector is described by the effective potential $\mathcal{U}\left(\Phi, \bar{\Phi}; T\right)$ chosen in order to reproduce the results obtained in lattice calculations. From the several possibilities, we use [14],

$$\frac{\mathcal{U}\left(\Phi, \bar{\Phi}; T\right)}{T^4} = -\frac{a\,(T)}{2}\bar{\Phi}\Phi + b(T) \times \ln[1 - 6\bar{\Phi}\Phi + 4(\bar{\Phi}^3 + \Phi^3) - 3(\bar{\Phi}\Phi)^2], \quad (2)$$

where

$$a\,(T) = a_0 + a_1\left(\frac{T_0}{T}\right) + a_2\left(\frac{T_0}{T}\right)^2 \text{ and } b(T) = b_3\left(\frac{T_0}{T}\right)^3. \quad (3)$$

The parameters for this effective potential are $a_0 = 3.51$, $a_1 = -2.47$, $a_2 = 15.2$, and $b_3 = -1.75$. T_0, the critical temperature for the deconfinement phase transition within pure gauge, can be fixed to $T_0 = 270$ MeV according to lattice findings. However, this value of T_0 leads to a difference between the chiral and deconfinement transition temperatures (indicating a week entanglement between both transitions), and also a larger value of the deconfinement temperature at a zero chemical potential than the value $T_c = 173 \pm 8$ MeV given by full LQCD data [30].

The extended version of the model where an effective four-quark vertex depending on the Polyakov loop is introduced, the entanglement-PNJL (EPNJL) model [16], allows the reduction of the difference between the transitions temperatures. We implement an explicit dependence of G_S on Φ and $\bar{\Phi}$ assuming the following form:

$$G_S(\Phi) = G_S^0\left[1 - \alpha_1\,\Phi\bar{\Phi} - \alpha_2\,(\Phi^3 + \bar{\Phi}^3)\right], \quad (4)$$

which respects chiral, P, C and the extended $\mathbb{Z}_3$ symmetries (the values $\alpha_1 = \alpha_2 = 0.2$ were fixed in [16]).

The Polyakov potential $\mathcal{U}$ may depend on μ ($\mu = \mu_q = (\mu_u + \mu_d)/2$) as a consequence of the backreaction of the fermion sector to the gluon sector. This dependence of $\mathcal{U}$ in μ can be introduced by a $T_0(\mu)$ which was estimated from renormalization-group arguments [17]:

$$T_0(\mu, N_f) = T_\tau e^{-\frac{1}{\alpha_0 b(\mu)}} \quad (5)$$

with $b(\mu) = (11N_c - 2N_f)/(6\pi) - 16N_f\mu^2/(\pi T_\tau^2)$, $\alpha_0 = 0.304$ and $T_\tau = 1.770$ (GeV). The value of T_0 also depends on N_f and in our case ($N_f = 2$) this leads to $T_0(\mu = 0, N_f) = 208$ MeV, with an uncertainty not small than ± 30 MeV [17].

From the Lagrangian (1) it is straightforward to obtain the PNJL grand potential density in the mean-field approximation, the constituent quark mass and the quark condensate, $\langle\bar{q}q\rangle$ (for a detailed description see [14,15]).

As a regularization procedure we use a sharp cutoff, Λ, in three-momentum space for all integrals. In the numerical calculations our parameters are: $m_0 = 6$ MeV, $\Lambda = 590$ MeV, and $G_S^0\Lambda^2 = 2.435$ which give $M_q^{vac} = 400$ MeV, $m_\pi = 140.2$ MeV, $f_\pi = 92.6$ MeV [18]. We will use $T_0(\mu = 0, N_f = 2) = 179$ MeV, that is the lower limit of the estimation of $T_0(\mu = 0, N_f = 2)$, which allows the transition temperature for the desconfinement to be close to the LQCD value. $T_0(\mu, N_f = 2)$ will follow Eq. (5).

3 Phase diagram, the location of the CEP and isentropic trajectories

The phase diagram is plotted in Fig. 1 and is determined by the grand canonical potential dependence on the order parameters $\langle\bar{q}q\rangle$, Φ and $\bar{\Phi}$ as a function of temperature and chemical potential. The deconfinement transition is defined as $\partial^2\Phi/\partial T^2 = 0$ (dotted lines)[1] while the crossover line is defined as $\partial^2\langle\bar{q}q\rangle/\partial T^2 = 0$ (dashed lines).

At $\mu = 0$ the deconfinement transition and the chiral crossover almost coincide at $T = 185$ MeV. At finite T and

[1] We could also represent $\partial^2\bar{\Phi}/\partial T^2 = 0$ but we will restrict ourselves to $\partial^2\Phi/\partial T^2 = 0$.

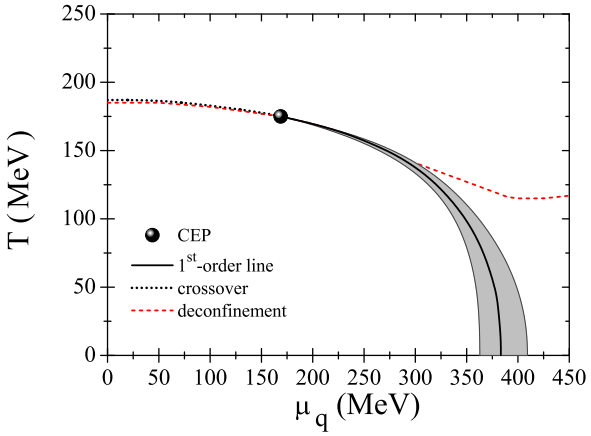

Fig. 1. QCD phase diagram in the $T-\mu_q$ plane. The red dashed line corresponds to the deconfinement transition. The full black line is the first order chiral phase transition and the gray region is the spinodal region.

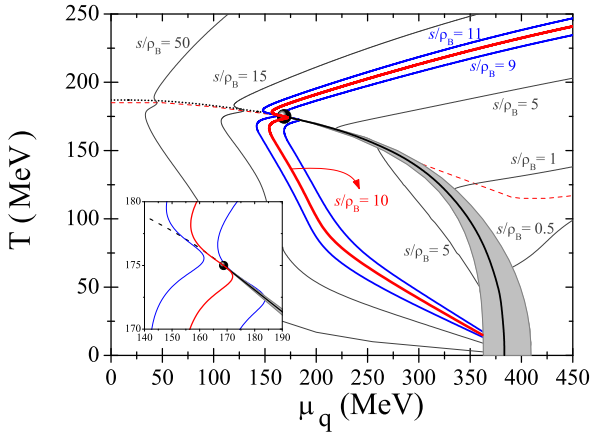

Fig. 2. Isentropic trajectories in the $T-\mu_q$ plane.

μ the deconfinement transition and the chiral crossover stay almost coincident (see red and black dashed lines, respectively) until the CEP is reached at ($T^{CEP} = 175$ MeV; $\mu_q^{CEP} = 169$ MeV). When $T = 0$, with the chosen parametrization, the first order phase transition occurs at $\mu_q^{crit} = 383$ MeV. As $\mu_q^{crit} < M_q^{vac}$ this allows for the existence of quark droplets (states in mechanical equilibrium with the vacuum state, $\rho_B = 0$, at $P = 0$) [18].

The isentropic lines (contours of constant entropy per baryon s/ρ_B) contain important information on the adiabatic evolution of the system. This has important consequences in HIC because the expansion of the QGP, which is accepted to be an hydrodynamic expansion of an ideal fluid, will nearly follow trajectories of constant entropy. Indeed, the fast (local) thermalization time and the good agreement of the data at RHIC with ideal relativistic hydrodynamic models (assuming a fluid evolution with zero viscosity) have been presented as evidences that the matter formed at RHIC is a strongly interacting QGP [19]. Due to its relevance, we investigate the isentropic lines crossing the chiral phase transition around the CEP in both the crossover and first order transitions.

The results for the isentropic lines in the $(T-\mu_q)$ plane are shown in Fig. 2. We first analyse the behavior of the isentropic lines in the limit $T \to 0$. As already pointed out, our model allows for the existence of quark droplets, and, in addition, simple thermodynamic behavior in the limit $T \to 0$ are verified. Indeed, in this limit $s \to 0$ according to the third law of thermodynamics and the condition $s/\rho_B = const.$ is satisfied [20]. Near the first order region, the isentropic lines with $s/\rho_B \lesssim 4$ come from the region of partial restored chiral symmetry and reach directly the phase transition region going then along with it as T decreases until it reaches $T = 0$. The isentropic lines with $4 \lesssim s/\rho_B \lesssim 10$ intersect the first order line and go over it for a while. Then, they leave the first order region through the chirally broken phase and they will reach the first order region again for higher (lower) values of μ (T). The trajectory with $s/\rho_B = 10$ arrives to the first order line very close the CEP and shows a pronounced kink behavior, a "focusing" effect already found in [21]. The same happens to the case of $s/\rho_B = 11$ (the CEP acts as an attractor of isentropic trajectories [21]).

In the crossover region the isentropic trajectories have slight kink behaviors when crossing the transition and they reach the first order region from lower values of μ_q. For isentropic lines $s/\rho_B \approx 50$ the kink almost disappears and the trajectories have a qualitatively similar behavior to the one obtained in lattice calculations [22].

All trajectories directly terminate at the same point of the horizontal axes at $T = 0$: as the temperature decreases the first order phase transition occurs, the latent heat increases and the formation of the mixed phase is thermodynamically favored.

4 π and σ-mesons properties around the CEP

We can obtain additional information about the phase diagram by calculating the masses of the pion and the sigma mesons, m_π and m_σ, as functions of T and μ_q. These masses, are obtained by using the standard mesonic polarization functions Π_π and Π_σ (see [23] for details).

At $T = \mu_q = 0$ the pion is a bound state, but, as the temperature increases it will dissociate in a $\bar{q}q$ pair (when $M_\pi > 2M_q$) at the Mott temperature. The polarization operator acquires an imaginary part and the resonance m_π has an associated decay width. The sigma is always a resonance and dissociates in a $\bar{q}q$ for all temperatures[2].

The behavior of the masses of the chiral partners (π, σ) at $(T \neq 0, \mu_q = 0)$ and at $(T = 0, \mu_q \neq 0)$ are qualitatively similar and well known from the literature: they both converge at a certain value of the temperature (chemical potential). This is known as the *effective* restoration

[2] We make the zero width approximation and only take the real part of the polarization operators [25].

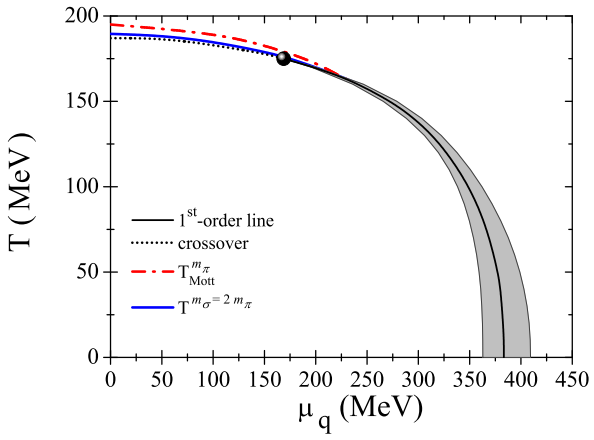

Fig. 3. The chiral phase transition, the line where $m_\sigma = 2m_\pi$ (blue line), and the Mott line for the pion (red dot-dashed line) in the $T - \mu_q$ plane.

of chiral symmetry and can also be seen by the merging of the π and σ spectral functions [15]. For $T \neq 0$ and $\mu_q = 0$ the degeneracy of the chiral partners occurs in a range of temperatures where the mesons are no longer bound states. Since the pion dissociates in $\bar{q}q$ pair, in Fig. 3 we represent the respective "Mott line" (red dot-dashed line). Above $\mu_q \approx 401$ MeV the "Mott line" occurs inside the first order region. Due to its relevance for the $\sigma \to \pi\pi$ process we also plot in Fig. 3 the threshold of this decay defined by $m_\sigma(T,\mu) = 2m_\pi(T,\mu)$ (blue line).

One interesting aspect is that, around the CEP, the σ-meson can have an abnormally small mass. This means that it is expected that some peculiar experimental signatures can be observed through its spectral changes. In fact, in hot and dense media the σ-meson can decay through different processes like $\sigma \to \pi\pi$, $\sigma \to \gamma\gamma$, etc. We will focus on the $\sigma \to \pi\pi$ decay but we will not consider the Bose-Einstein statistics for the final state pions because, as pointed out in [24], this effect at high temperatures is gradually washed out as μ_q increases.

Near the chiral transition temperature, m_σ is significantly reduced while m_π increases making impossible the σ-meson decay into two pions and, therefore, the width coming from this process vanishes being the threshold point of the decay defined by $m_\sigma(T,\mu) = 2m_\pi(T,\mu)$. Indeed, in the chiral limit the threshold $m_\sigma(T,\mu) = 2m_\pi(T,\mu)$ must coincide with the restoration of chiral symmetry because at that point $M_q = m_0$ and $m_\sigma(T,\mu) = m_\pi(T,\mu)$. Outside the chiral limit, M_q goes asymptotically to m_0 and at the transition temperature $M_q >> m_0$: both phenomena do not coincide, but they occur near each other.

Once we assume the σ-meson as a quark-antiquark pair, the decay width for the $\sigma \to \pi\pi$ process is:

$$\Gamma_{\sigma\to\pi\pi} = \frac{3}{2}\frac{g^2_{\sigma\pi\pi}}{16\, m_\sigma}\sqrt{1 - \frac{4\, m_\pi^2}{m_\sigma^2}}, \qquad (6)$$

where $g_{\sigma\pi\pi}(T,\mu) = 2g_\sigma g_\pi^2 A_{\sigma\pi\pi}(T,\mu)$ is the coupling strength. g_σ and g_π are coupling constants for the σ and π-mesons respectively, and $A_{\sigma\pi\pi}$ is the amplitude of the triangle vertex for the decay $\sigma \to \pi\pi$ (see details in [24,26, 27]). The constraint $m_\sigma(T,\mu) \leq 2m_\pi(T,\mu)$ comes from the factor $\sqrt{1 - 4m_\pi^2/m_\sigma^2}$ in Eq. (6). When $m_\sigma(T,\mu) > 2m_\pi(T,\mu)$ the values $g_{\sigma\pi\pi}$ and $\Gamma_{\sigma\to\pi\pi}$ will go to zero.

In Fig. 4 we present the behavior of $\Gamma_{\sigma\to\pi\pi}$ and $g_{\sigma\pi\pi}$ as functions of the temperature for 3 cases:
Case I $-$ $\mu_q = 0$;
Case II $-$ $\mu_q = \mu_q^{CEP}$ and $\mu_q = \mu_q^{CEP} \pm 30$ MeV;
Case III $-$ $s/\rho_B = 9$ (the isentropic line reaches the first order phase transition from the chirally symmetric phase); $s/\rho_B = 10$ (the isentropic line passes very close the CEP; $s/\rho_B = 11$ (the isentropic line goes through the crossover and intersects the first order line from below).

In Case I (Fig. 4, left panel), at $T = 0$, we have $m_\sigma = 803.8$ MeV which gives $g_{\sigma\pi\pi} = 2.73$ GeV, slightly above the experimental value extracted from the J/ψ decays given by the BES collaboration: $g_{\sigma\pi\pi} = 2.0^{+0.3}_{-0.9}$ GeV [28]. When the temperature increases $g_{\sigma\pi\pi}$ drops to zero near the point $m_\sigma = 2m_\pi$. For the $\sigma \to \pi\pi$ decay, we obtain $\Gamma_{\sigma\to\pi\pi} = 260$ MeV, within the certainty intervals of the experimental results from the BES collaboration $\Gamma_{\sigma\to\pi\pi} = 282^{+77}_{-50}$ MeV (with $m_\sigma = 390^{+60}_{-36}$ MeV), or the E791 Collaboration with $\Gamma_{\sigma\to\pi\pi} = 324^{+40}_{-42} \pm 21$ MeV (with $m_\sigma = 478^{+24}_{-23} \pm 17$ MeV) [29]. As noticed in [24], the choice of parameters can make shifts of magnitudes in $g_{\sigma\pi\pi}$ and $\Gamma_{\sigma\to\pi\pi}$, mainly due to the value of m_σ, but does not change their shapes, especially the behavior around the threshold temperature or the chiral transition.

In Case II, around the CEP, (Fig. 4, middle panel) the result is very similar to what was found in [24,26]: as the chemical potential increases close to the CEP, the threshold temperature the for σ decay decreases. In the first-order transition region ($\mu_q = \mu_q^{CEP} + 30$ MeV) $\langle\bar{q}q\rangle$, m_π and m_σ are discontinuous: $\langle\bar{q}q\rangle$ and m_σ jump down and m_π jumps up and, consequently, the mass difference between m_π and m_σ jumps from below $2m_\pi$ to above $2m_\pi$. The σ decay threshold coincides with the first-order transition line and $g_{\sigma\pi\pi}$ and $\Gamma_{\sigma\to\pi\pi}$ go to zero. At the CEP ($\mu_q = \mu_q^{CEP}$) the limiting threshold for the σ decay approximately coincides with the temperature of the CEP, T^{CEP} (see red line for $g_{\sigma\pi\pi}$ and $\Gamma_{\sigma\to\pi\pi}$). In the crossover region ($\mu_q = \mu_q^{CEP} - 30$ MeV), $g_{\sigma\pi\pi}$ and $\Gamma_{\sigma\to\pi\pi}$ go to zero slightly above the temperature where $\partial^2\langle\bar{q}q\rangle/\partial T^2 = 0$. This is due to the continuous nature of the transition in this region and the way we define the crossover.

In Case III, we impose that the decay $\sigma \to \pi\pi$ occurs in the isentropic trajectories (Fig. 4, right panel). The location of the CEP is not known yet, but, it can be argued in favor of its experimental detection that if the evolution of strongly interacting matter is such that the system passes in the vicinity of the CEP starting from the initial conditions we will be able to locate it. Due to the successes of ideal fluid hydrodynamics at RHIC, it is likely that the system expands nearly isentropically and the $\sigma \to \pi\pi$ decay, if it occurs, will be under such conditions.
$-$ For $s/\rho_B = 9$ (dashed lines) $g_{\sigma\pi\pi}$ and $\Gamma_{\sigma\to\pi\pi}$ drop to zero and there is a range, $176 < T < 184$ MeV, where the

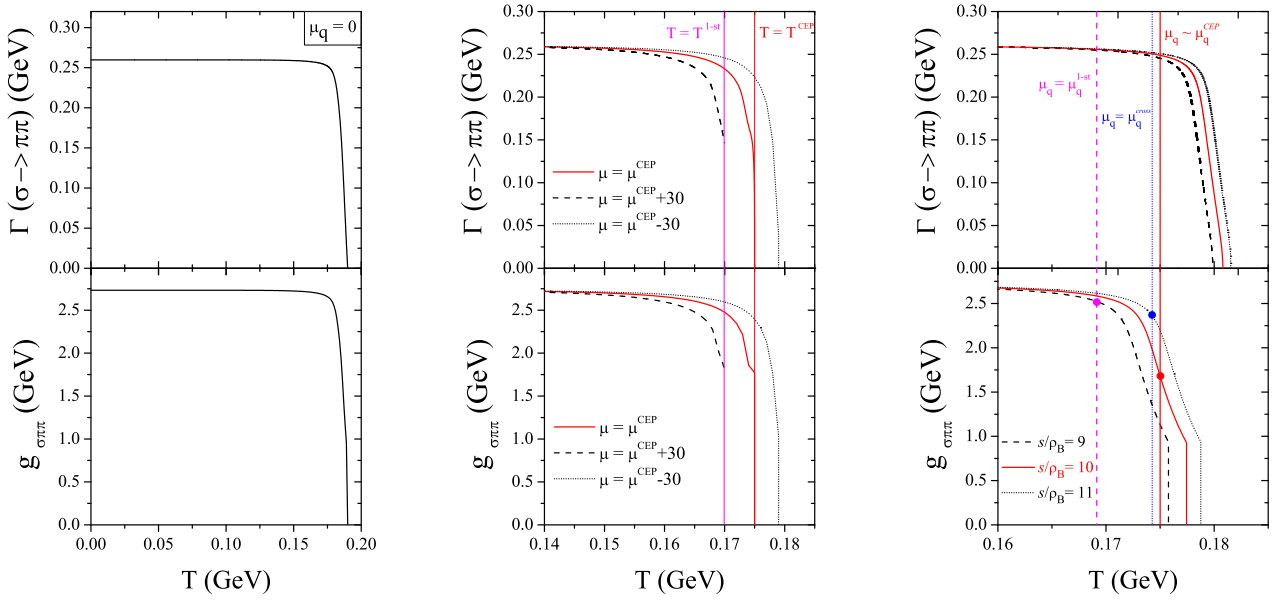

Fig. 4. $\Gamma_{\sigma\to\pi\pi}$ (upper panels) and $g_{\sigma\pi\pi}$ (lower panels) for the three cases presented: Case I ($\mu_q = 0$), left panels; Case II ($\mu_q = \mu_q^{CEP}$, $\mu_q^{CEP} \pm 30$), middle panels; Case III ($s/\rho_B = 9, 10, 11$), right panels.

$\sigma \to \pi\pi$ decay occurs inside the first order region and we do not have decays for temperatures and chemical potentials above the first order line.
– When $s/\rho_B = 11$ (dotted lines) $g_{\sigma\pi\pi}$ and $\Gamma_{\sigma\to\pi\pi}$ will be different from zero slightly above the isentropic line reaches the crossover transition as T decreases. The $\sigma \to \pi\pi$ decay then occurs until $T \approx 14$ MeV and for $T < 14$ MeV it will be inside the first order region.
– For $s/\rho_B = 10$ (solid red line) the trajectory passes very close to the CEP. $g_{\sigma\pi\pi} = 1.67$ GeV and $\Gamma_{\sigma\to\pi\pi} = 135$ MeV in the point near the CEP. Both quantities go to zero inside the region of chiral restored phase but near the transition line.

When the $\sigma \to \pi\pi$ decay occurs at the transition lines, for these values of s/ρ_B, $g_{\sigma\pi\pi}$ and $\Gamma_{\sigma\to\pi\pi}$ are smaller when it occurs near the CEP: the red dot (at the CEP) in Fig. 4, right panel, has a smaller value compared with the magenta dot (crossover) and the blue dot (first order).

The $\sigma \to \pi\pi$ decay depends on the initial conditions and the way the system evolves after the thermalization. If the isentropic trajectories reach the first order line for $\mu_q > \mu_q^{1st}$, there will be no pions coming from the σ decay in the chirally symmetric phase. Near the CEP and above the $\sigma \to \pi\pi$ decay is possible and its width is still high near the CEP.

5 Summary

The location of the CEP is one important issue addressed by the HIC program. The Nuclotron-based Ion Collider Facility at JINR will significantly enhance our understanding of the QCD phase diagram namely the nature of the phase transition and the existence/location of the CEP. The eventual confirmation of the CEP would be one of the first discoveries of QCD-like observables in the medium. The implications of its location are vast, in particular concerning the constraints to set on effective models.

In this work we started to study the isentropic lines in the vicinity of the CEP. The isentropic trajectories, in the crossover region very close the CEP, show "focusing" effects which can be seen as the result of the CEP to act as an attractant of isentropic trajectories [21]). At high chemical potentials and low temperatures these lines will go through the first order line.

By taking into account the π and σ-mesons properties around the CEP, we looked for signatures that can be observed experimentally [6]. We have focused on the $\sigma \to \pi\pi$ decay that can be suppressed at the transition region due to the small mass the σ-meson can have in that region. This decay showed different behaviors concerning the region where the collision takes place and may be used to distinguish different transition types and to locate the CEP: if the isentropic trajectories reach the first order region coming from higher temperatures, only after the transition the $\sigma \to \pi\pi$ decay happens and no pions from σ decay occur in the chirally symmetric phase. Otherwise, if the isentropic trajectories reach the crossover, pions coming from σ decay may still occur in the chirally symmetric phase.

Acknowledgment: I would like to thank J. Moreira and C. Providência for helpful discussions. This work was supported by "Fundação para a Ciência e Tecnologia", Portugal, under the Grant No. SFRH/BPD/1022 73/2014.

References

1. M. K. Volkov, E. A. Kuraev, D. Blaschke, G. Ropke and S. M. Schmidt, Phys. Lett. B **424** (1998) 235.
2. P. Rehberg, Y. L. Kalinovsky and D. Blaschke, Nucl. Phys. A **622** (1997) 478.
3. `http://nica.jinr.ru/files/BM@N/BMN_CDR.pdf`.
4. B. I. Abelev *et al.* [STAR Collaboration], Phys. Rev. C **81** (2010) 024911.
5. L. Adamczyk *et al.* [STAR Collaboration], Phys. Rev. Lett. **113** (2014) 092301.
6. T. Anticic *et al.* [NA49 Collaboration], Phys. Rev. C **81** (2010) 064907.
7. M. Gazdzicki [NA49 and NA61/SHINE Collaborations], J. Phys. G **38** (2011) 124024.
8. Y. Akiba *et al.*, arXiv:1502.02730 [nucl-ex].
9. P. Costa, M. Ferreira, H. Hansen, D. P. Menezes and C. Providência, Phys. Rev. D **89** (2014) 056013.
10. P. Costa, M. Ferreira, D. P. Menezes, J. Moreira and C. Providência, Phys. Rev. D **92** (2015) 036012.
11. K. Fukushima, Phys. Rev. D **77** (2008) 114028.
12. K. Fukushima, Phys. Rev. C **67** (2003) 025203.
13. T. Hatsuda, T. Kunihiro and H. Shimizu, Phys. Rev. Lett. **82** (1999) 2840.
14. C. Ratti, M. A. Thaler and W. Weise, Phys. Rev. D **73** (2006) 014019.
15. H. Hansen, W. M. Alberico, A. Beraudo, A. Molinari, M. Nardi and C. Ratti, Phys. Rev. D **75** (2007) 065004.
16. Y. Sakai, T. Sasaki, H. Kouno and M. Yahiro, Phys. Rev. D **82** (2010) 076003.
17. T. K. Herbst, J. M. Pawlowski and B. J. Schaefer, Phys. Lett. B **696** (2011) 58.
18. M. Buballa, Phys. Rept. **407** (2005) 205.
19. D. G. d'Enterria, J. Phys. G **34** (2007) S53.
20. P. Costa, H. Hansen, M. C. Ruivo and C. A. de Sousa, Phys. Rev. D **81** (2010) 016007.
21. C. Nonaka and M. Asakawa, Phys. Rev. C **71** (2005) 044904.
22. S. Ejiri, F. Karsch, E. Laermann and C. Schmidt, Phys. Rev. D **73** (2006) 054506.
23. T. Hatsuda and T. Kunihiro, Phys. Rept. **247** (1994) 221.
24. P. Zhuang and Z. Yang, Phys. Rev. D **63** (2001) 016004.
25. T. Hatsuda and T. Kunihiro, Prog. Theor. Phys. Suppl. **91** (1987) 284.
26. A. V. Friesen, Y. L. Kalinovsky and V. D. Toneev, Phys. Part. Nucl. Lett. **9** (2012) 1.
27. J. Hufner, S. P. Klevansky, E. Quack and P. Zhuang, Phys. Lett. B **337** (1994) 30.
28. N. Wu, hep-ex/0104050.
29. E. M. Aitala *et al.* [E791 Collaboration], Phys. Rev. Lett. **86** (2001) 770.
30. F. Karsch, E. Laermann and A. Peikert, Nucl. Phys. B **605** (2001) 579.